Title

Microfluidic filter device with nylon mesh membranes efficiently dissociates cell aggregates and digested tissue into single cells

Journal

Lab on a Chip, 18(18)

ISSN

1473-0197

Authors

Qiu, Xiaolong
Lombardo, Jeremy A
Westerhof, Trisha M
et al.

Publication Date

2018-09-11

DOI

10.1039/c8lc00507a

Peer reviewed

HHS Public Access

Author manuscript

Lab Chip. Author manuscript; available in PMC 2019 September 11.

Published in final edited form as:

Lab Chip. 2018 September 11; 18(18): 2776–2786. doi:10.1039/c8lc00507a.

Microfluidic filter device with nylon mesh membranes efficiently dissociates cell aggregates and digested tissue into single cells

Xiaolong Qiu[#a], **Jeremy A. Lombardo**[#a], **Trisha M. Westerhof**[d], **Marissa Pennell**[a], **Anita Ng**[a], **Hamad Alshetaiwi**[e], **Brian M. Luna**[a], **Edward L. Nelson**[c,d,f], **Kai Kessenbrock**[e,f], **Elliot E. Hui**[a,g], and **Jered B. Haun**[*,a,b,f,g]

[a.]Department of Biomedical Engineering, University of California Irvine, Irvine, CA 92697, USA.

[b.]Department of Chemical Engineering and Materials Science, University of California Irvine, Irvine, CA 92697, USA.

[c.]Department of Medicine, Division of Hematology/Oncology, School of Medicine, University of California, Irvine, Irvine, CA 92697, USA

[d.] Department of Molecular Biology and Biochemistry, School of Biological Sciences, University of California, Irvine, Irvine, CA 92697, USA.

[e.]Department of Biological Chemistry, School of Medicine, University of California, Irvine, Irvine, CA, 92697, USA.

[f.]Chao Family Comprehensive Cancer Center, University of California Irvine, Irvine, CA 92697, USA.

[g.]Center for Advanced Design and Manufacturing of Integrated Microfluidics, University of California, Irvine, Irvine, CA, 92697, USA.

[#] These authors contributed equally to this work.

Abstract

Tissues are increasingly being analyzed at the single cell level in order to characterize cellular diversity and identify rare cell types. Single cell analysis efforts are greatly limited, however, by the need to first break down tissues into single cell suspensions. Current dissociation methods are inefficient, leaving a significant portion of the tissue as aggregates that are filtered away or left to confound results. Here, we present a simple and inexpensive microfluidic device that simultaneously filters large tissue fragments and dissociates smaller aggregates into single cells, thereby improving single cell yield and purity. The device incorporates two nylon mesh membranes with well-defined, micron-sized pores that operate on aggregates of different size scales. We also designed the device so that the first filtration could be performed under tangential

[*]Jered B. Haun, PhD, Department of Biomedical Engineering, University of California Irvine, 3107 Natural Sciences II, Irvine, CA, 92697, Phone: 949-824-1243, jered.haun@uci.edu, http://haun.eng.uci.edu.

Author Contributions

X.Q., M.P., E.E.H., and J.B.H. devised the concept for the work. M.P. and B.M.L. fabricated prototypes of the device. X.Q., J.A.L., T.M.W., M.P., A.N., and H.A. carried out the experimental work. X.Q., J.A.L, T.M.W., E.L.N., K.K., E.E.H., and J.B.H. carried out the experimental analysis. X.Q., J.A.L., and J.B.H. wrote the paper.

Conflicts of interest

There are no conflicts to declare.

flow to minimize clogging. Using cancer cell lines, we demonstrated that aggregates were effectively dissociated using high flow rates and pore sizes that were smaller than a single cell. However, pore sizes that were less than half the cell size caused significant damage. We then improved results by passing the sample through two filter devices in series, with single cell yield and purity predominantly determined by the pore size of the second membrane. Next, we optimized performance using minced and digested murine kidney tissue samples, and determined that the combination of 50 and 15 μm membranes was optimal. Finally, we integrated these two membranes into a single filter device and performed validation experiments using minced and digested murine kidney, liver, and mammary tumor tissue samples. The dual membrane microfluidic filter device increased single cell numbers by at least 3-fold for each tissue type, and in some cases by more than 10-fold. These results were obtained in minutes without affecting cell viability, and additional filtering would not be required prior to downstream applications. In future work, we will create complete tissue analysis platforms by integrating the dual membrane microfluidic filter device with additional upstream tissue processing technologies, as well as downstream operations such as cell sorting and detection.

Abstract

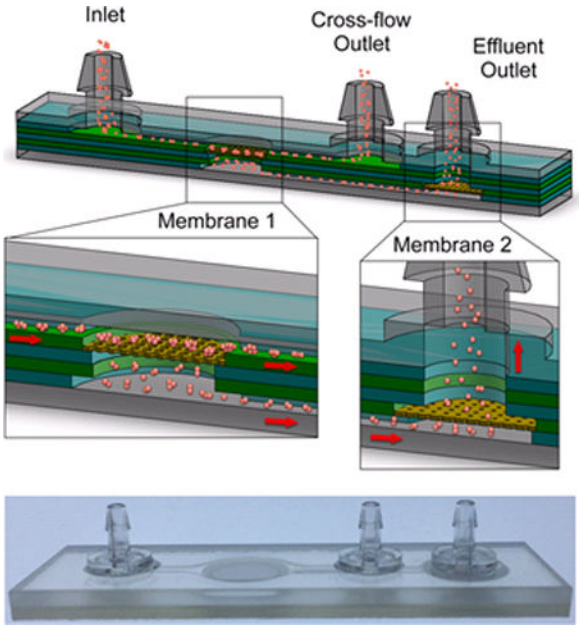

Keywords

microfluidics; tissue; filtration; dissociation; single cell

Introduction

Complex tissues are increasingly being analyzed at the single cell level in an effort to catalogue diversity and identify rare driver cells. This would provide a comprehensive cell census that could be used to better understand tissue or organ biology, as promoted by the Human Cell Atlas initiative,[1–3], as well as improve the diagnosis and treatment of major

diseases including solid tumors.[4–10] Cell-based diagnostic methods such as flow cytometry, mass cytometry, and single cell RNA sequencing are ideally positioned to meet the above goals,[11–14] but a major limitation is the need to first break tissue down into a suspension of single cells.[12]. Traditionally, tissue has been dissociated by mincing into small pieces with a scalpel, digesting with proteolytic enzymes, mechanically dissociating with a pipetter and/or vortexing, and filtering with a cell strainer to remove remaining aggregates. Microfluidic technologies have recently been developed to automate and improve tissue dissociation, including on-chip digestion[15,16] and disaggregation using sharp surface edges, post arrays, and branching channel networks that generate hydrodynamic fluid jets.[17–20] While these devices have improved processing speed and single cell yield, small aggregates invariably remain after processing. Eliminating these aggregates by enhancing dissociation power or providing an on-chip separation mechanism would improve the quality of single cell suspensions and enable immediate downstream analysis.

Large tissue fragments and cell aggregates are commonly removed from digested tissue samples using cell strainers that contain nylon mesh filters with pore sizes ranging from 35–80 μm. These pores are large enough to allow small aggregates and clusters to pass through along with the single cells. While cell strainers with smaller pore sizes are available, they are typically not used due to concerns over the loss of single cells. Placing the filter membranes within a microfluidic device should alleviate this issue by minimizing hold-up volume and improving wash efficiency. Moreover, a microfluidic filter device that could be operated at high flow rate (>10 mL/min) could be directly integrated with previously developed hydrodynamic tissue digestion and aggregate dissociation technologies.[16,19,20] Vacuum-driven filtration systems containing track-etched membranes,[21–23] and microfluidic devices containing microfabricated membranes,[24–28] have been described. These works primarily focused on size-based separation of single cells, typically larger circulating tumor cells (CTCs) from smaller blood cells. Pore sizes ranged from 5–10 μm to capture CTCs, and flow rates ranged from mL/hr for whole blood to 10 mL/min for diluted blood. In addition to size, cell deformability was shown to affect filtration, as cells could extrude through smaller pores depending on their viscosity and the flow rate.[23] Regarding cell aggregates, a novel microfabricated pillar array was designed to capture intact CTC clusters,[29] which have been correlated with higher metastatic potential and worse prognosis relative to individual CTCs.[30,31] The CTC Cluster-Chip successfully trapped >90% of cancer cell line aggregates containing 5 or more cells when operated at 2.5 ml/h, but performance eroded quickly as aggregate size decreased and flow rate increased. This was superior to a track-etched membrane with 5 μm pores, presumably because cell clusters were able to squeeze through the pores. To date, the fate of single cells or cell clusters that pass through microporous membranes has not been investigated. Moreover, nylon membranes similar to those used in cell strainers have not been evaluated within a microfluidic device. These nylon membranes are commercially available as single layer woven meshes with excellent pore density and uniformity down to 5 μm diameter.

In this work, we integrate nylon mesh membranes with pore sizes ranging from 5 to 50 μm into laser micro-machined, laminated plastic devices and investigate the filtration of tissue fragments, cell aggregates, and single cells. Devices are designed to operate under a traditional direct filtration mode, with sample passing through the membrane, or a tangential

filtration mode that utilizes a cross-flow to prevent membrane clogging (Fig. 1). Using cancer cell lines, we first show that nylon membranes with 10 μm pores or smaller remove all aggregates containing four or more cells, even when operated at high flow rates (mL/min). However, some clusters of 2 to 3 cells still pass through pores that are as small as 5 μm. Interestingly, we observe that single cell numbers increase significantly after passing pore sizes that are smaller than the cells, by as much as five-fold, but this is also correlated with cell damage. We also show that dissociation is only weakly dependent on flow rate through the membrane, but is significantly diminished by the presence of a cross-flow under tangential filtration mode. We then enhance single cell recovery and purity by coupling two filter devices in series, such that aggregates are progressively dissociated into smaller sizes. Results predominantly correlate with the pore size of the second membrane, which is smaller and invariably used in direct filtration mode. Next, we optimize performance using minced and digested murine kidney tissue samples, and demonstrate that the combination of 50 and 15 μm pore size membranes produces the most single cells. Finally, we integrate the 50 and 15 μm pore size membranes into a single microfluidic device and validate results using murine kidney, liver, and mammary tumor tissue samples. After mincing and digesting with collagenase, the dual membrane filter device increases single cell yield by at least 3-fold, and in some cases by more than 10-fold, while also maintaining cell viability and reducing aggregates. Most strikingly, using the device after a brief 15 min digestion produces as many single cells as a 60 min digestion. Reducing processing time in this manner would help preserve cell viability, phenotype, and molecular signatures for subsequent molecular analysis. Our simple and inexpensive microfluidic filter device significantly improves the recovery of single cells from tissue, and we envision future integration with upstream tissue processing technologies, such as our hydro-mincing and branching channel array, to maximize dissociation speed and efficiency.

Results and Discussion

Device Design

We designed our microfluidic filter device to remove tissue fragments and cell aggregates produced by standard enzymatic digestion procedures or comparable microfluidic processing.[16] This would enhance single cell purity for downstream diagnostic applications, and any aggregates that were retained could be further processed to increase overall cell recovery. A schematic of the device is shown in Fig. 1A. Sample is introduced via the inlet and comes into contact with a microporous membrane. Sample that passes through the membrane will exit through the effluent outlet. A portion of the sample can also be directed along the surface of the membrane and exit through the cross-flow outlet. This arrangement was chosen to maximize device utility by enabling operation in either direct and tangential filtration modes. Under direct filtration, all sample would pass through the membrane to maximize sample recovery and processing speed. Under tangential flow, the cross-flow would sweep larger tissue fragments and cell aggregates away from the membrane surface to prevent clogging. However, not all of the sample would be filtered, requiring multiple passes to collect the full sample.

Filter devices were fabricated using a commercial laminate approach, with channel features laser micro-machined into hard plastic (polyethylene terephthalate, PET). This provides a more robust end-product than alternative fabrication methods, such as photolithography and casting of polydimethyl siloxane (PDMS), and thus better supports the high flow rates and pressures that are desired for rapid tissue filtration. A total of seven PET layers were used, including two channel layers, three via layers, and two layers to seal the device (Fig. 1B). We included two locations for mounting thin, microporous membranes. The first location was in the center of the device, sandwiched between the middle channel and top via layers, and this membrane would be used for either tangential or direct filtration of large tissue fragments and cellular aggregates. We hypothesized that a second membrane with smaller pores could help maximize single cell purity. This membrane was placed immediately upstream of the effluent outlet, sandwiched between the bottom channel and second via layers, and would allow for direct filtration of smaller aggregates and clusters. Hose barbs were mounted in the top layer to serve as device inlets and outlets. After laser micro-machining, devices were assembled by stacking the various layers and membranes together, which were then firmly bonded using adhesive and pressure lamination. Channel height was ~300 μm, which included contributions from the plastic (250 μm) and adhesive (~50 μm).

For the microporous membranes, we chose to utilize single-layer, woven nylon meshes similar to those used in cell strainers. These are commercially available with pore sizes down to 5 μm from numerous vendors as inexpensive, ready-to-use sheets that can be cut to size. The nylon threads create a lattice network with high pore density and uniformity, which should limit back-pressure and allow for high flow rates through the membrane. Micrographs of the nylon mesh membranes used in this study are shown in Fig. 1C, and properties are listed in Table 1. Moreover, we hypothesized that the narrow cross-section and rounded shape of the nylon threads will be ideal for dissociating aggregates into smaller clusters or even single cells. This is similar in principle to the sharp silicon edges of the Biogrid device,[17] but now operating on a large scale and, importantly, avoiding costly microfabrication. We would expect a dissociation mechanism to be most prevalent when aggregates are only slightly larger than the pores. Aggregates that span many pores are more likely to be captured in a manner similar to traditional filtration. Track-etched membranes were considered, as they are also cheap, easy to use, and have been used extensively in single cell and aggregate filtration studies.[21–23,29] However, the largest pore size available is 30 μm, and the random localization of the pores can cause them to overlap, particularly at high porosity. Microfabricated membranes offer precise control over pore size, shape, and location and have been used for cell filtration and compartmentalization.[24–28,32] However, custom fabrication adds cost and complexity. Finally, pores within both track etched and microfabricated membranes are defects within the material, making them less durable at high porosity. For nylon mesh membranes, tensile forces will be resisted by the threads and dissipated throughout the material, making them more robust and failure-resistant. Thus, we concluded that nylon mesh membranes provided the optimal combination of cost and performance characteristics, while also providing potential for aggregate dissociation. A fabricated microfluidic filter device containing two nylon mesh membranes is shown in Fig. 1D.

Filtration of cell line aggregates

We first investigated single cell recovery and viability for nylon mesh membranes with 5, 10, 15, 25, or 50 μm pore sizes. To eliminate confounding effects, we fabricated devices containing only the first membrane (see Membrane 1 in Fig. 1A). Experiments were performed using MCF-7 human breast cancer cells, which are strongly cohesive and provide large numbers of aggregates from standard tissue culture. We also note that MCF-7 cells are very large at ~20 μm diameter. Cell suspensions were passed through devices using a syringe pump, and initial tests were performed using direct filtration at 12.5 mL/min. Device effluents were recovered and imaged under phase contract microscopy to identify single cells, clusters of 2 to 3 cells, small aggregates of 4 to 10 cells, and large aggregates of >10 cells. Recovery results for each population are plotted in Fig. 2A. Large and small aggregates constituted 10% and 15% of the control population, respectively. These percentages decreased after filtration, in concordance with pore size, down to <0.5% for the 5 and 10 μm pores. Single cells were initially present at less than 30%, and progressively rose as pore size decreased, reaching a maximum of 85%. Clusters remained around 40–45% for all but the 5 and 10 μm pore sizes, but even then were still present at a substantial level. We also quantified single cell numbers using a cell counter, and results are plotted in Fig. 2B after normalization by the control. For the 50 μm pore size, ~15% of single cells were lost, most likely due to holdup or non-specific adhesion within the device. For all other pore sizes, more single cells were recovered after filtration, suggesting that a percentage of the aggregate and/or cluster populations were dissociated into single cells. Dissociation became more pronounced as pore size decreased, with single cells increasing by more than 5-fold for the 5 μm pore size. However, extruding cells through smaller pores compromised viability, as determined by flow cytometry using a propidium iodide exclusion assay (Fig. 2C). Specifically, losses in viability scaled inversely with single cell recovery. As a result, the number of viable single cells that were recovered remained constant, around 40% higher than the control, for the 5, 10, and 15 μm pore sizes (see Supplementary Information, Fig. S1).

We next examined the effect of flow rate while still utilizing the direct filtration mode. We found that decreasing flow rate as low as 0.25 mL/min resulted in general trends toward lower single cell numbers and higher viability, but these changes were not significant (Fig. 2D-E). Aggregate, cluster, and single cell percentages were also similar for each flow rate (see Supplementary Information, Fig. S1). Finally, we investigated tangential filtration mode by diverting the sample between the cross-flow and effluent outlets using two syringe pumps that were operated in withdrawal mode. The total flow rate was held constant at 12.5 mL/min, similar to direct filtration experiments, while the cross-flow was varied from 40 to 80%. Afterwards, sample collected from the cross-flow outlet was passed through the membrane in direct filtration mode at 12.5 mL/min, and both effluents were combined prior to analysis. We found that single cell numbers were similar at all cross-flow ratios (Fig. 2F), which were significantly lower than direct filtration experiments at 12.5 mL/min (compare to Fig. 2B). In fact, single cell numbers under tangential filtration were similar to direct filtration at 0.25 mL/min, even though all tangential experiments were performed utilized higher membrane flow-through rates (>2.5 mL/min). We did find that tangential filtration removed large aggregates more effectively at the 50 μm pore size (see Supplementary

Information, Fig. S1). Taken together, we conclude that under pressure driven flow, aggregate and cluster dissociation depended primarily on membrane pore size and whether a cross-flow was present, and less so on the flow rate through the membrane.

Improving aggregate dissociation using two membranes

Based on these results, we postulated that aggregate dissociation could be enhanced by passing samples through two nylon membranes in series. In this scenario, the first membrane would reduce aggregate size such that the second membrane could better liberate single cells. Therefore, we coupled two single-membrane filter devices in series using tubing and performed direct filtration experiments at 12.5 mL/min. Since we were primarily interested in dissociation, we initially tested the smaller pore size membranes in various combinations. We found that passing MCF-7 suspensions through two filter devices eliminated nearly all aggregates (Fig. 3A), even for the 15 μm pore size. Clusters were also reduced relative to the single filter experiments (compare to Fig. 2A), reaching a low of 9% for the 5–5 membrane combination. Single cell number and viability results are presented in Fig. 3B and C, respectively. Single cell yield did not change for the 5–5 and 10–5 membrane combinations relative to the single filter case (compare to Fig. 2B), as samples were already well-dissociated. However, the 15–5 membrane combination produced fewer single cells, suggesting that the 15 μm membrane captured aggregates that the 5 μm membrane would have been able to dissociate into single cells. For the 10 μm membrane, single cell numbers were similar between single and double filter device experiments. The only case in which the use of two membranes was beneficial was for the 15–15 membrane combination, which increased single cell numbers increased from 50% to 150% higher than the control. We found that cell viability was predominantly determined by the pore size of the second, smaller membrane, and that values were similar to the single filter device experiments (compare to Fig. 2C). While we again observed that viability was generally correlated with single cell numbers, live single cell numbers were lowest for conditions that employed the 5 μm membrane (see Supplementary Information, Fig. S2). Thus, we deemed the 5 μm pores too small, at least for these ~20 μm MCF-7 cells. For the 10–10, 15–10, and 15–15 membrane combinations, live single cell recovery was ~60% higher than the control. For context, this level of dissociation is comparable to the best version of our branching channel dissociation device for the same MCF-7 cell model.[20]

Next, we investigated using the 10 and 15 μm membranes in combination with the larger 25 and 50 μm membranes. Two filter devices were coupled in series as previously described, but now experiments were performed under tangential filtration. As with single filter device experiments, total flow rate was held constant at 12.5 mL/min and sample collected from the cross-flow outlet was passed through both devices under direct filtration mode. Using 60% cross-flow, we found that single cell, cluster, and aggregate populations were similar to the direct flow experiments utilizing the same 10 and 15 μm membranes (Fig. 3D). However, a small number of aggregates were recovered from the 50–15 membrane combination. Single cell recovery and viability results were also generally determined by the second, smaller membrane (Fig. 3E and F). As such, single cell numbers for the 10 μm pore size were similar to direct flow experiments using either one or two filter devices. For the 15 μm pore size, single cell numbers were similar to the 15–15 membrane combination under direct

filtration, but now viability was significantly higher and equal to the control. It is unclear whether this change was related to using larger pore sizes in the upstream filter device, tangential filtration mode, or a combination of both. In total, live single cell numbers were ~2-fold greater than the control for all but the 25–15 combination (see Supplementary Information, Fig. S2). We note that nearly identical results were obtained for tangential filtration experiments performed using 80% cross-flow (see Supplementary Information, Fig. S2). Based on the combined results obtained with the MCF-7 cell aggregate model, we conclude that the second membrane predominantly dictated single cell recovery and viability because of its smaller pore size and consistent utilization of the direct filtration mode. Placing a second membrane upstream could improve results in some cases, particularly for the 15 μm membrane, but the pore size and operational mode of the first membrane was less important.

Optimization using murine kidney tissue

Since our ultimate goal is to use the filter devices with complex tissues, we next evaluated performance using murine kidney tissue samples. We continued to use two filter devices in series, specifically the larger 25 or 50 μm pore sizes followed by smaller 10 or 15 μm pore sizes. The first filtration was performed under direct or tangential (60% cross-flow) mode, and a total flow rate of 12.5 mL/min. Fresh kidneys were harvested, sliced into histologically similar sections with a scalpel, minced into ~1 mm^3 pieces, and weighed. Samples were then digested with collagenase and mechanically treated by vortexing and pipetting, per routine protocol. We initially evaluated device performance using tissue samples that were only briefly digested with collagenase, as this would prove the most stringent test of membrane clogging and dissociation power. After digestion for 15 min, device treatment increased single cell numbers by at least 2-fold for all membrane combinations and filtration modes (Fig. 4A). Maximal results were ~4-fold higher than control, which were obtained for both 25 μm pore size combinations under direct filtration and both 50 μm pore size combinations under tangential filtration. Increasing digestion time to 30 min enhanced single cell recovery for all device conditions, which were now at least 5-fold higher than the control (Fig. 4B). Results were generally greater for the 15 μm pore combinations regardless of the first membrane size or operational mode, which was consistent with our findings with the MCF-7 aggregate model. For both 15 and 30 min digestion times, we observed that large pieces of tissue were trapped by the first membrane (Fig. 4A), but membrane fouling was not an issue for either direct or tangential filtration modes, most likely because we were using relatively small tissue samples (<100 mg).

Based on these preliminary results, we chose to further evaluate cell suspensions using flow cytometry. Specifically, we used a panel of stains to assess cell viability and identify red blood cells and leukocytes, as we have previously described.[16,20] We also chose to only use the 50 μm pore size in the first device due to higher porosity and the direct filtration mode since it was faster and easier to execute. The number of single tissue cells recovered per mg tissue is shown in Fig. 4C. Results at the 15 and 30 min digestion times were similar to the cell counter data in Figs. 4A and B, with both 50–10 and 50–15 membrane combinations producing 5- to 10-fold more single cells than the control. Digesting for 60 min resulted in a dramatic increase in single tissue cell numbers to ~20,000/mg. The 50–10 membrane

combination was similar to the control, but the 50–15 membrane combination enhanced recovery by 2.5-fold. Notably, the 50–15 membrane combination also produced similar numbers of single tissue cells after digesting for 15 min as the control after digesting for 60 min. Cell viability was ~90% for all conditions at the 15 and 30 min digestion time points (Fig. 4D). However, 60 min digestion decreased viability to ~80% for the control and ~75% for the 50–15 μm filter combination. We also used scattering information to quantify the percentage of aggregates relative to single cells (Fig. 4E). We note that samples were passed through a 35 μm cell strainer prior to analysis to prevent clogging of the cytometer, and thus results likely only reflect cell clusters. Aggregate percentage increased progressively with digestion time for controls, from 3 to 11%, indicating that traditional dissociation methods are not effective at reducing tissue all the way down to single cells. Aggregate percentages remained unchanged for the 50–15 membrane combination, but the 50–10 membrane combination reduced aggregates by approximately half at the 30 and 60 min digestion time points. Red blood cell and leukocyte recoveries are shown in the Supplementary Information (see Supplementary Information, Fig. S3), and closely mirrored the single tissue cell recovery results in Fig. 4C.

Filter device integration and validation using murine organ and tumor tissues

Based on the superior performance of the 50–15 membrane combination in terms of single tissue cells recovered from kidney samples, we fabricated a single device containing both membranes, as shown in Fig. 1. The double membrane filter device was first validated using murine kidney samples that were digested for 60 min, and performance in terms of single tissue cell recovery and viability was comparable to the previous results obtained with two single filter devices coupled in series (see Supplementary Information, Fig. S3). We then tested freshly resected murine liver samples, which are generally easier to enzymatically digest, but hepatocytes are also well-known to be fragile.[16] After a brief 15 min digestion, approximately 2500 single tissue cells were obtained per mg liver tissue for the control, and this was enhanced 5-fold by filter device treatment (Fig. 5A). At 30 min, single tissue cells increased by 2-fold for the control, but device treatment remained static, resulting in a more modest 2-fold improvement. Both control and device conditions were both much higher after 60 min digestion, around 40,000 single tissue cells/mg, indicating that the liver tissue had been fully broken down by enzymatic digestion. Viability remained greater than 90% for all conditions (Fig. 5B), which was very encouraging considering the fragile nature of hepatocytes. Aggregates were present at ~1% for controls at all digestion times, and were generally reduced by device treatment although differences were not significant (Fig. 5C). As a final evaluation, we used mammary tumors that spontaneously arise in MMTV-PyMT transgenic mice. Tumors are generally considered among the most difficult epithelial tissues to dissociate due to their abnormal extracellular matrix composition.[33] For these tests, we modified the flow cytometry detection panel by adding an antibody specific for the general epithelial marker EpCAM. This enabled us to positively identify epithelial tissue cells, although this would include both normal or cancerous cells. Control conditions produced ~1000 single epithelial cells per mg tumor tissue at both the 15 and 30 min digestion time points, and this only increased to ~2000 cells/mg after 60 min digestion (Fig. 5D). Device treatment enhanced single cell recovery by approximately 3-fold at all time points. Epithelial cell viability was only ~40–50% for all conditions (Fig. 5E), potentially indicating that the

tumor samples contained highly necrotic regions. A significant number of aggregates were present at all conditions, in the range of 15–20% of the total recovered population (Fig. 5F). This suggests that more dissociation power will be needed to effectively liberate all cells from tumors. For both liver and tumor samples, red blood cell and leukocyte recoveries followed similar trends as the single liver tissue cell and single epithelial cell data (see Supplementary Information, Fig. S4).

Conclusions

In this work, we have presented a simple and inexpensive microfluidic filter device that can rapidly and effectively improve the quality of single cell suspensions obtained from digested tissue samples. This was accomplished using nylon mesh membranes with well-defined, micron-scale pores that simultaneously filtered larger tissue fragments and dissociated smaller aggregates into single cells. Specifically, we demonstrated that using two nylon mesh membranes, first a larger pore size in the range of 25–50 μm followed by a smaller pore size in the range of 10–15 μm, resulted in dissociation of aggregates into progressively smaller sizes and ultimately enhanced single cell recovery. The dissociation effect was likely due to the combination of hydrodynamic shear forces and physical interaction with the nylon threads. While this was effective, we note that care must be given to prevent cell damage, particularly for complex tissues that may contain cells of different sizes. Using the final dual membrane microfluidic filter device with 50 and 15 μm pore sizes, the number of single cells recovered from minced and digested murine kidney, liver, and tumor tissue samples was enhanced by at least 3-fold, and in some cases by more than 10-fold. We also showed that a brief 15 min digestion and filter device treatment could produce comparable single cell numbers to a full 60 min digestion. Importantly, cell viability was maintained for all tissue types and operating conditions, even fragile liver cells. These results will be important for advancing single cell analysis and atlasing of complex tissues, as dissociation has been a major bottleneck hindering these efforts.[12] Improved mechanical dissociation efficiency would help by reducing manual labor and enzyme cost, ensuring that sufficient sample is recovered even from smaller clinical specimens, and preventing bias in the final suspension towards cells that are easiest to isolate. Alternatively, shorter digestion times would accelerate tissue processing work flows and could potentially better preserve the original phenotypic state from within the tissue. While we used nylon mesh membranes in this study, it is possible that track etched or microfabricated membranes with similar pore sizes could provide similar results. Our design also included the option to perform the first filtration under tangential mode, although this was not found to be critical for generating single cells. We do note that it is possible that tangential filtration could become more important if tissue size were scaled up beyond 100 mg. Additionally, cell aggregates could be passed through the filter device continuously to increase single cell recovery, similar to diafiltration.[34] In future work, we will continue to optimize the microfluidic filter device using different tissue types. We will also integrate the filter device with our hydro-mincing digestion device to enable automated processing of cm-scale tissue samples,[16] as well as our branching channel dissociation device to maximize single cell numbers and purity.[19,20] This integrated platform would be capable of processing full tissue samples all the way down to a highly pure suspension of single cells in a rapid and efficient manner. Furthermore, we will seek to

integrate downstream technologies to enable on-chip sorting and analysis of single cells to create point-of-care diagnostic platforms for tissue samples.

Experimental

Device fabrication.

Microfluidic devices were fabricated by ALine, Inc. (Rancho Dominguez, CA). Briefly, fluidic channels, vias, and openings for membranes and hose barb were etched into polyethylene terephthalate (PET) layers using a CO_2 laser. Nylon mesh membranes were purchased from Amazon Small Parts (10, 15, 25, and 50 μm pore sizes; Seattle, WA) or EMD Millipore (5 μm; Burlington, MA) as large sheets and were cut to size using the CO_2 laser. Device layers, nylon mesh membranes, and hose barbs were then assembled, bonded using adhesive, and pressure laminated to form a single monolithic device.

Cell culture aggregate model and murine tissue samples.

MCF-7 human breast cancer cell line was purchased from ATCC (Manassas, VA). Cells were cultured at 37°C and 5% CO_2 in tissue culture flasks using DMEM media containing 10% FBS, non-essential amino acids, 1 mM sodium pyruvate, 2 mM L-Glutamine, 100 μg/mL streptomycin, 100 U/mL penicillin, and 44U/L Novolin R insulin (Thermo Fisher, Waltham, MA). Prior to experiments, confluent monolayers were briefly digested for 5 min with trypsin-EDTA, which released cells with a substantial number of aggregates. Cell suspensions were then centrifuged and resuspended in PBS containing 1% BSA (PBS+). Kidneys and liver were harvested from freshly sacrificed BALB/c or C57B/6 mice (Jackson Laboratory, Bar Harbor, ME) that were determined to be waste from a research study approved by the University of California, Irvine's Institutional Animal Care and Use Committee (courtesy of Dr. Angela G. Fleischman). Mammary tumors were harvested from freshly sacrificed MMTV-PyMT mice (Jackson Laboratory, Bar Harbor, ME). For kidneys, a scalpel was used to prepare ~1 cm long x ~1 mm diameter strips of tissue, each containing histologically similar portions of the medulla and cortex. Each tissue strip was then further minced with a scalpel to ~1 mm^3 pieces. Liver and mammary tumors were uniformly minced with a scalpel to ~1 mm^3 pieces. Minced tissue samples were then weighed, placed within microcentrifuge tubes along with 300 μL of 0.25% collagenase type I (Stemcell Technologies, Vancouver, BC), digested at 37°C in a shaking incubator under gentle agitation for 15, 30, or 60 min, and mechanically disaggregated by repeated pipetting and vortexing. Finally, cell suspensions were treated with 100 Units of DNase I (Roche, Indianapolis, IN) for 10 min at 37°C and washed by centrifugation into PBS+.

Dissociation and filtration studies.

Microfluidic filter devices were prepared by affixing 0.05" ID tubing (Saint-Gobain, Malvern, PA) to the device inlet and outlet hose barbs. Prior to experiments, devices were incubated with SuperBlock (PBS) blocking buffer (Thermo Fisher Scientific, Waltham, MA) at room temperature for 15 min to reduce non-specific binding of cells to the membranes and channel walls and washed with PBS+. MCF-7 cells or digested murine tissue samples were loaded into a syringe and passed through the device using a syringe pump (Harvard Apparatus, Holliston, MA) at total flow rates ranging from 0.25 to 12.5 mL/min. For

tangential filtration experiments, two syringe pumps were employed in withdrawal mode, one each connected to the cross-flow and effluent outlets. The withdrawal rates were adjusted to achieve a given cross-flow rate, while total flow rate was always maintained at 12.5 mL/min. Following the initial pass, sample collected from the cross-flow outlet was passed directly through the membrane at 12.5 mL/min and collected from the effluent outlet. Following all experiments, devices were washed with 1 mL PBS+ to flush out any remaining cells, and all effluents were combined into a single sample. Cell counts were obtained using a Moxi Z automated cell counter and type S cassettes (Orflo, Hailey, ID).

Quantifying cell aggregates by microscopy.

Single cells and aggregates were assessed by microscopy using methods that we previously described.[20] Briefly, MCF-7 cell suspensions were imaged with a Hoffman phase contrast microscope and a 4x objective. Raw images were then converted to binary using MATLAB, and ImageJ was used to identify, outline, and calculate the area of all contiguous cellular units. Each unit was then classified based on area as a single cell (20 to 80 pixels^2 or 75 to 300 μm^2), cluster (80 to 200 pixels^2 or 300 to 750 μm^2), small aggregate (200 to 300 pixels^2 or 750 to 1120 μm^2), or large aggregate (>300 pixels^2 or >1120 μm^2). Referencing back to the micrographs, this corresponded to ~2 to 3 cells for clusters, ~4–10 cells for small aggregates, and >10 cells for large aggregates.

Flow cytometry.

We closely followed the flow cytometry protocol that we previously developed for tissue suspensions.[16] Briefly, cell suspensions were co-stained with 2.5μg/mL anti-mouse CD45-PE monoclonal antibody (clone 30-F11, BioLegend, San Diego, CA) and 0.5X CellMask Green (Thermo Fisher, Waltham, MA) for 20 minutes at 37°C. Samples were then washed twice using PBS+ by centrifugation, co-stained with 5 μg/mL 7-AAD (BD Biosciences, San Jose, CA) and 12.5 μM DRAQ5 (BioLegend) on ice for at least 15 minutes, and analyzed on an Accuri C6 Flow Cytometer (BD Biosciences). Flow cytometry data was compensated and analyzed using FlowJo software (FlowJo, Ashland, OR), and a sequential gating scheme was used to identify live and dead single tissue cells from leukocytes, red blood cells, non-cellular debris, and cellular aggregates.

Statistics.

Data are represented as the mean ± standard error. Error bars represent the standard error from at least three independent experiments. P-values were calculated from at least three independent experiments using students t-test.

Supplementary Material

Refer to Web version on PubMed Central for supplementary material.

Acknowledgements

The authors would like to thank Dr. Angela G. Fleischman for kindly donating mouse kidney and liver tissues. We would also like to thank Danny Duong, Dalia Hammouri, and Miami Shafeeq for assisting with experiments and/or image analysis. Funding support was received from the National Science Foundation and the industrial members of

the Center for Advanced Design and Manufacturing of Integrated Microfluidics (NSF I/UCRC award number IIP-1362165), the Chan Zuckerberg Initiative, an advised fund of Silicon Valley Community Foundation, under the Human Cell Atlas project number 173894, the University of California's Cancer Research Coordinating Committee under award number CRC-15–380519, and the National Cancer Institute of the National Institutes of Health under Award Number P30CA062203. The content is solely the responsibility of the authors and does not necessarily represent the official views of the National Institutes of Health or National Science Foundation.

References

1. Rozenblatt-Rosen O, Stubbington MJT, Regev A and Teichmann SA, Nature, 2017, 550, 451–3. [PubMed: 29072289]
2. Regev A, Teichmann SA, Lander ES, Amit I, Benoist C, Birney E, Bodenmiller B, Campbell P, Carninci P, Clatworthy M, Clevers H, Deplancke B, Dunham I, Eberwine J, Eils R, Enard W, Farmer A, Fugger L, Göttgens B, Hacohen N, Haniffa M, Hemberg M, Kim S, Klenerman P, Kriegstein A, Lein E, Linnarsson S, Lundberg E, Lundeberg J, Majumder P, Marioni JC, Merad M, Mhlanga M, Nawijn M, Netea M, Nolan G, Pe'er D, Phillipakis A, Ponting CP, Quake S, Reik W, Rozenblatt-Rosen O, Sanes J, Satija R, Schumacher TN, Shalek A, Shapiro E, Sharma P, Shin JW, Stegle O, Stratton M, Stubbington MJT, Theis FJ, Uhlen M, van Oudenaarden A, Wagner A, Watt F, Weissman J, Wold B, Xavier R, Yosef N and C. A. M. P. Human, Elife, 2017, 6,
3. Villani AC, Satija R, Reynolds G, Sarkizova S, Shekhar K, Fletcher J, Griesbeck M, Butler A, Zheng S, Lazo S, Jardine L, Dixon D, Stephenson E, Nilsson E, Grundberg I, McDonald D, Filby A, Li W, De Jager PL, Rozenblatt-Rosen O, Lane AA, Haniffa M, Regev A and Hacohen N, Science, 2017, 356,
4. Li X, Ling V and Li PC, Anal Chem, 2008, 80, 4095–102. [PubMed: 18447319]
5. Li X, Chen Y and Li PC, Lab Chip, 2011, 11, 1378–84. [PubMed: 21327253]
6. Patel AP, Tirosh I, Trombetta JJ, Shalek AK, Gillespie SM, Wakimoto H, Cahill DP, Nahed BV, Curry WT, Martuza RL, Louis DN, Rozenblatt-Rosen O, Suvà ML, Regev A and Bernstein BE, Science, 2014, 344, 1396–401. [PubMed: 24925914]
7. Lawson DA, Bhakta NR, Kessenbrock K, Prummel KD, Yu Y, Takai K, Zhou A, Eyob H, Balakrishnan S, Wang CY, Yaswen P, Goga A and Werb Z, Nature, 2015, 526, 131–5. [PubMed: 26416748]
8. Tirosh I, Izar B, Prakadan SM, Wadsworth MH, Treacy D, Trombetta JJ, Rotem A, Rodman C, Lian C, Murphy G, Fallahi-Sichani M, Dutton-Regester K, Lin JR, Cohen O, Shah P, Lu D, Genshaft AS, Hughes TK, Ziegler CG, Kazer SW, Gaillard A, Kolb KE, Villani AC, Johannessen CM, Andreev AY, Van Allen EM, Bertagnolli M, Sorger PK, Sullivan RJ, Flaherty KT, Frederick DT, Jané-Valbuena J, Yoon CH, Rozenblatt-Rosen O, Shalek AK, Regev A and Garraway LA, Science, 2016, 352, 189–96. [PubMed: 27124452]
9. Li H, Courtois ET, Sengupta D, Tan Y, Chen KH, Goh JJL, Kong SL, Chua C, Hon LK, Tan WS, Wong M, Choi PJ, Wee LJK, Hillmer AM, Tan IB, Robson P and Prabhakar S, Nat. Genet, 2017,
10. Venteicher AS, Tirosh I, Hebert C, Yizhak K, Neftel C, Filbin MG, Hovestadt V, Escalante LE, Shaw ML, Rodman C, Gillespie SM, Dionne D, Luo CC, Ravichandran H, Mylvaganam R, Mount C, Onozato ML, Nahed BV, Wakimoto H, Curry WT, Iafrate AJ, Rivera MN, Frosch MP, Golub TR, Brastianos PK, Getz G, Patel AP, Monje M, Cahill DP, Rozenblatt-Rosen O, Louis DN, Bernstein BE, Regev A and Suvà ML, Science, 2017, 355, [PubMed: 28126774]
11. Bendall SC and Nolan GP, Nat. Biotechnol, 2012, 30, 639–47. [PubMed: 22781693]
12. Gawad C, Koh W and Quake SR, Nat. Rev. Genet, 2016, 17, 175–88. [PubMed: 26806412]
13. Kolodziejczyk AA, Kim JK, Svensson V, Marioni JC and Teichmann SA, Mol. Cell, 2015, 58, 610–20. [PubMed: 26000846]
14. Stubbington MJT, Rozenblatt-Rosen O, Regev A and Teichmann SA, Science, 2017, 358, 58–63. [PubMed: 28983043]
15. Hattersley SM, Dyer CE, Greenman J and Haswell SJ, Lab Chip, 2008, 8, 1842–6. [PubMed: 18941683]
16. Qiu X, Westerhof TM, Karunaratne AA, Werner EM, Pourfard PP, Nelson EL, Hui EE and Haun JB, Lab Chip, 2017, 17, 3300–9. [PubMed: 28850139]

17. Wallman L, Akesson E, Ceric D, Andersson PH, Day K, Hovatta O, Falci S, Laurell T and Sundstrom E, Lab Chip, 2011, 11, 3241–8. [PubMed: 21850297]
18. Lin CH, Lee DC, Chang HC, Chiu IM and Hsu CH, Anal. Chem, 2013, 85, 11920–8. [PubMed: 24228937]
19. Qiu X, De Jesus J, Pennell M, Troiani M and Haun JB, Lab Chip, 2015, 15, 339–50. [PubMed: 25377468]
20. Qiu X, Huang JH, Westerhof TM, Lombardo JA, Henrikson KM, Pennell M, Pourfard PP, Nelson EL, Nath P and Haun JB, Sci. Rep, 2018, 8, 2774. [PubMed: 29426941]
21. Vona G, Sabile A, Louha M, Sitruk V, Romana S, Schütze K, Capron F, Franco D, Pazzagli M, Vekemans M, Lacour B, Bréchot C and Paterlini-Bréchot P, Am. J. Pathol, 2000, 156, 57–63. [PubMed: 10623654]
22. Krebs MG, Hou JM, Sloane R, Lancashire L, Priest L, Nonaka D, Ward TH, Backen A, Clack G, Hughes A, Ranson M, Blackhall FH and Dive C, J. Thorac. Oncol, 2012, 7, 306–15. [PubMed: 22173704]
23. Coumans FA, van Dalum G, Beck M and Terstappen LW, PLoS One, 2013, 8, e61774. [PubMed: 23658615]
24. Zheng S, Lin H, Liu JQ, Balic M, Datar R, Cote RJ and Tai YC, J. Chromatogr. A, 2007, 1162, 154–61. [PubMed: 17561026]
25. Didar TF, Li K, Veres T and Tabrizian M, Biomaterials, 2013, 34, 5588–93. [PubMed: 23628474]
26. Zhou MD, Hao S, Williams AJ, Harouaka RA, Schrand B, Rawal S, Ao Z, Brenneman R, Gilboa E, Lu B, Wang S, Zhu J, Datar R, Cote R, Tai YC and Zheng SY, Sci. Rep, 2014, 4, 7392. [PubMed: 25487434]
27. Fan X, Jia C, Yang J, Li G, Mao H, Jin Q and Zhao J, Biosens. Bioelectron, 2015, 71, 380–6. [PubMed: 25950932]
28. Kang YT, Doh I, Byun J, Chang HJ and Cho YH, Theranostics, 2017, 7, 3179–91. [PubMed: 28900503]
29. Sarioglu AF, Aceto N, Kojic N, Donaldson MC, Zeinali M, Hamza B, Engstrom A, Zhu H, Sundaresan TK, Miyamoto DT, Luo X, Bardia A, Wittner BS, Ramaswamy S, Shioda T, Ting DT, Stott SL, Kapur R, Maheswaran S, Haber DA and Toner M, Nat. Methods, 2015, 12, 685–91. [PubMed: 25984697]
30. Hou JM, Krebs MG, Lancashire L, Sloane R, Backen A, Swain RK, Priest LJ, Greystoke A, Zhou C, Morris K, Ward T, Blackhall FH and Dive C, J. Clin. Oncol, 2012, 30, 525–32. [PubMed: 22253462]
31. Aceto N, Toner M, Maheswaran S and Haber DA, Trends Cancer, 2015, 1, 44–52. [PubMed: 28741562]
32. Kim MY, Li DJ, Pham LK, Wong BG and Hui EE, J. Memb. Sci, 2014, 452, 460–9. [PubMed: 24567663]
33. Paszek MJ and Weaver VM, J. Mammary Gland Biol. Neoplasia, 2004, 9, 325–42. [PubMed: 15838603]
34. Liu JF, Yadavali S, Tsourkas A and Issadore D, Lab Chip, 2017, 17, 3796–803. [PubMed: 29043350]

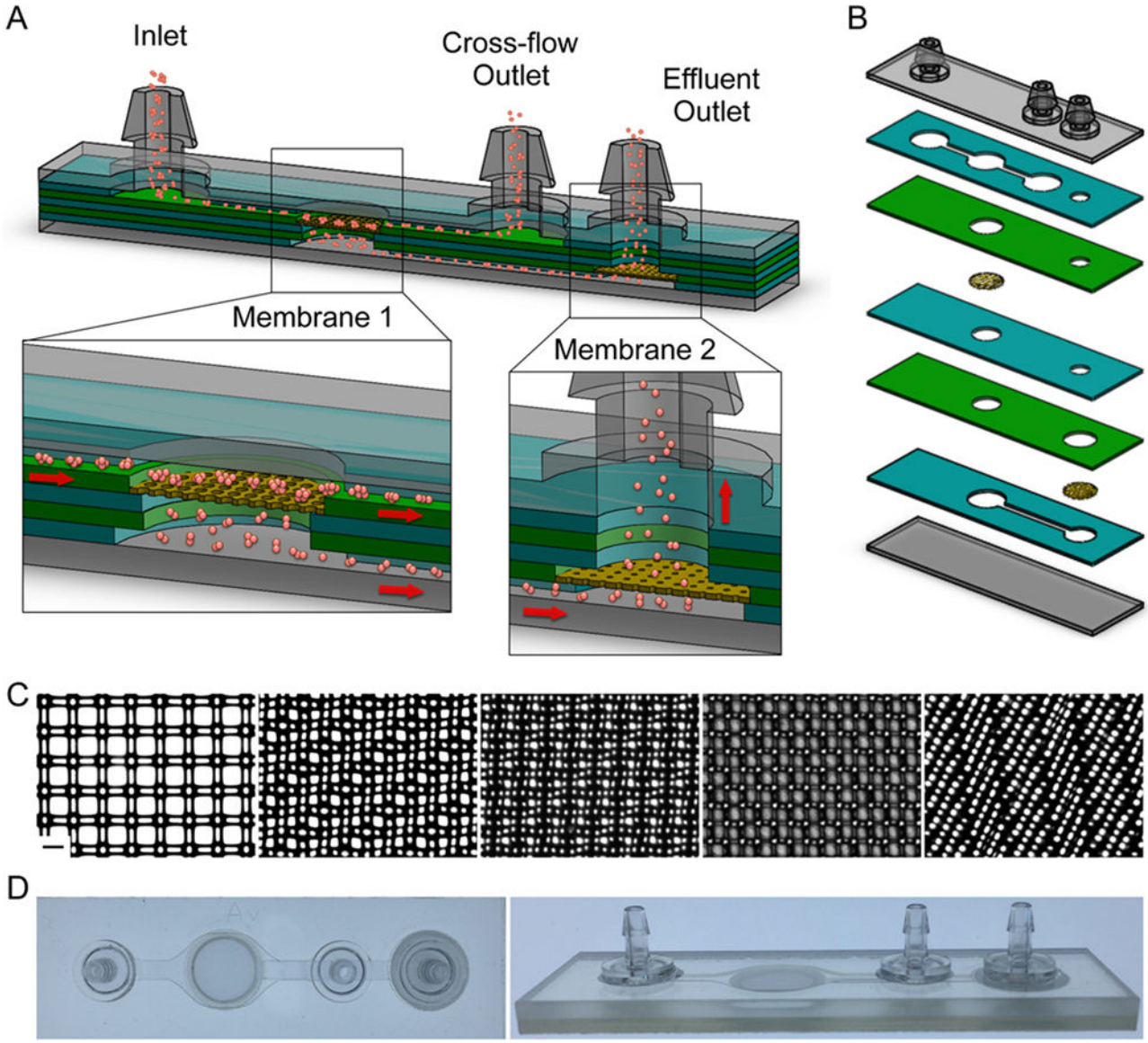

Figure 1. Microfluidic filter device for tissue specimens.

(A) Schematic of the microfluidic filter device containing two microporous membranes. The first membrane is located in the center of the device, and is intended to restrict large tissue fragments and aggregates from passing through to the Effluent Outlet (Direct Filtration). If desired, some of the sample can be passed over the surface of the first membrane for collection from the Cross-flow Outlet (Tangential Filtration). The second membrane is immediately upstream of the Effluent Outlet, and is intended to restrict smaller aggregates from reaching the Effluent Outlet. (B) Exploded view showing seven PET layers, including three channel layers, two via layers, and two layers to seal the top and bottom of the device (C) Micrographs of nylon mesh membranes, showing lattice network with high pore density and uniformity. Pore sizes are (left to right) 50, 25, 15, 10, and 5 μm diameter. (D) Top and side view of fabricated microfluidic filter device containing two nylon mesh membranes. Scale bar is 50 μm.

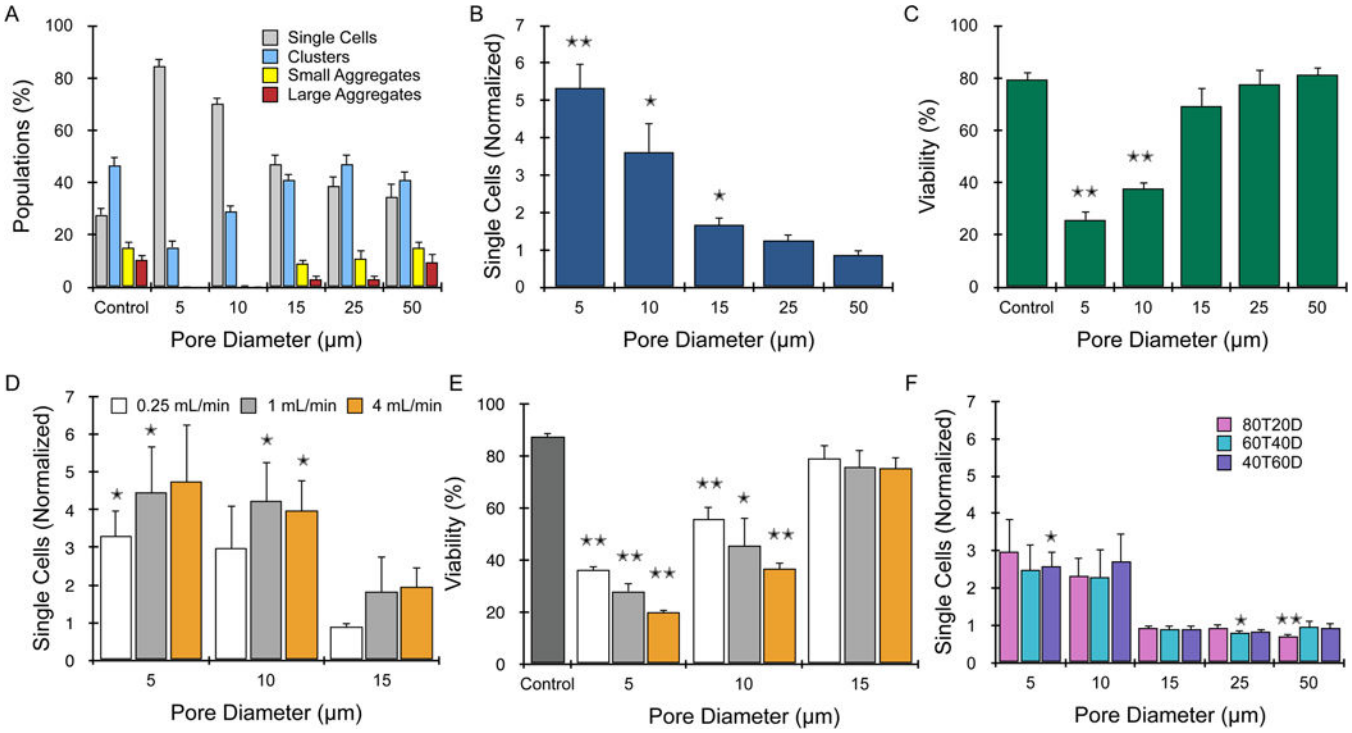

Figure 2. Characterization of single membrane filter devices using MCF-7 cells.

(A) Single cells, clusters, and aggregates were quantified from micrographs and plotted as percent of total population before (control) and after passing through filter devices containing one membrane with the indicated pore size. Devices were operated in direct filtration mode using a flow rate of 12.5 mL/min. Aggregates and clusters were removed with increasing efficiency as pore size decreased, with single cells starting at less than 30% and reaching a maximum of 85%. (B) Single cell numbers were quantified using a cell counter and normalized by the control. Significantly more single cells were recovered following filtration through the 5, 10, and 15 μm pore sizes, indicating dissociation of aggregates into single cells. (C) Viability was determined by propidium iodide exclusion assay, and decreased with pore size. (D,E) Direct flow experience at lower flow rates, which generally resulted in (D) less single cell number and (E) higher viability, although changes were modest. (F) Tangential filtration experiments using different cross-flow ratios (40 to 80%), which resulted in substantially lower single cell numbers than direct flow experiments at 12.5 mL/min. Error bars represent standard errors from at least three independent experiments. * indicates $p < 0.05$ and ** indicates $p < 0.01$ relative to the control.

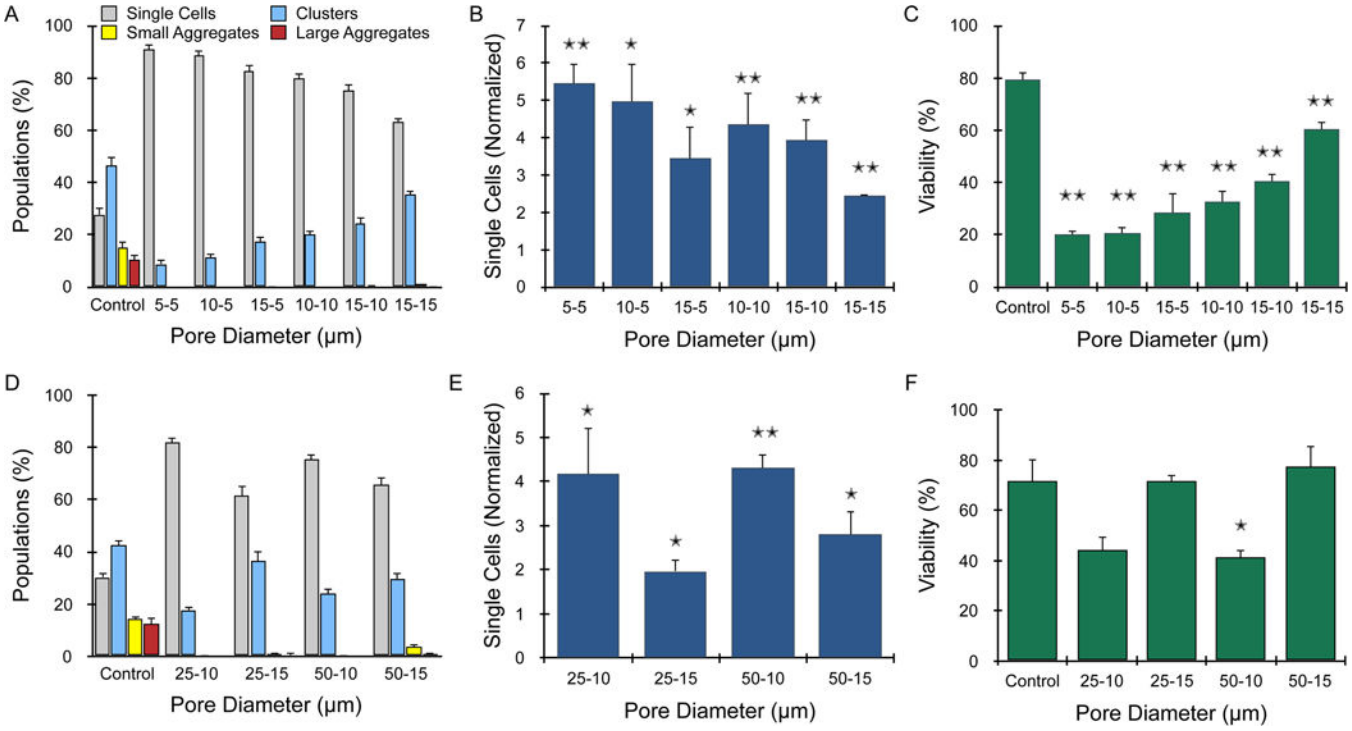

Figure 3. Combining two filter devices in series.

(A-C) Various combinations of the 5, 10, and 15 μm membrane filter devices were connected by tubing and operated under direct filtration mode at 12.5 mL/min flow rate. (A) Large and small aggregate populations were eliminated from all filter device combinations. (B) Single cell recovery and (C) viability were generally similar to the single filter, direct filtration experiments for the 5 and 10 μm membranes. The 15–15 membrane device combination did have higher single cell numbers than the 15 μm pore membrane alone. (D-F) Tangential filtration experiments using the 25 or 50 μm membranes followed by the 10 or 15 μm membranes with 60% cross-flow and 12.5 mL/min total flow rate. Results for (D) single cell, cluster, and aggregate populations, (E) single cell recovery, and (F) viability were all dictated primarily by the pore size of the second membrane. Error bars represent standard errors from at least three independent experiments. * indicates $p < 0.05$ and ** indicates $p < 0.01$ relative to the control.

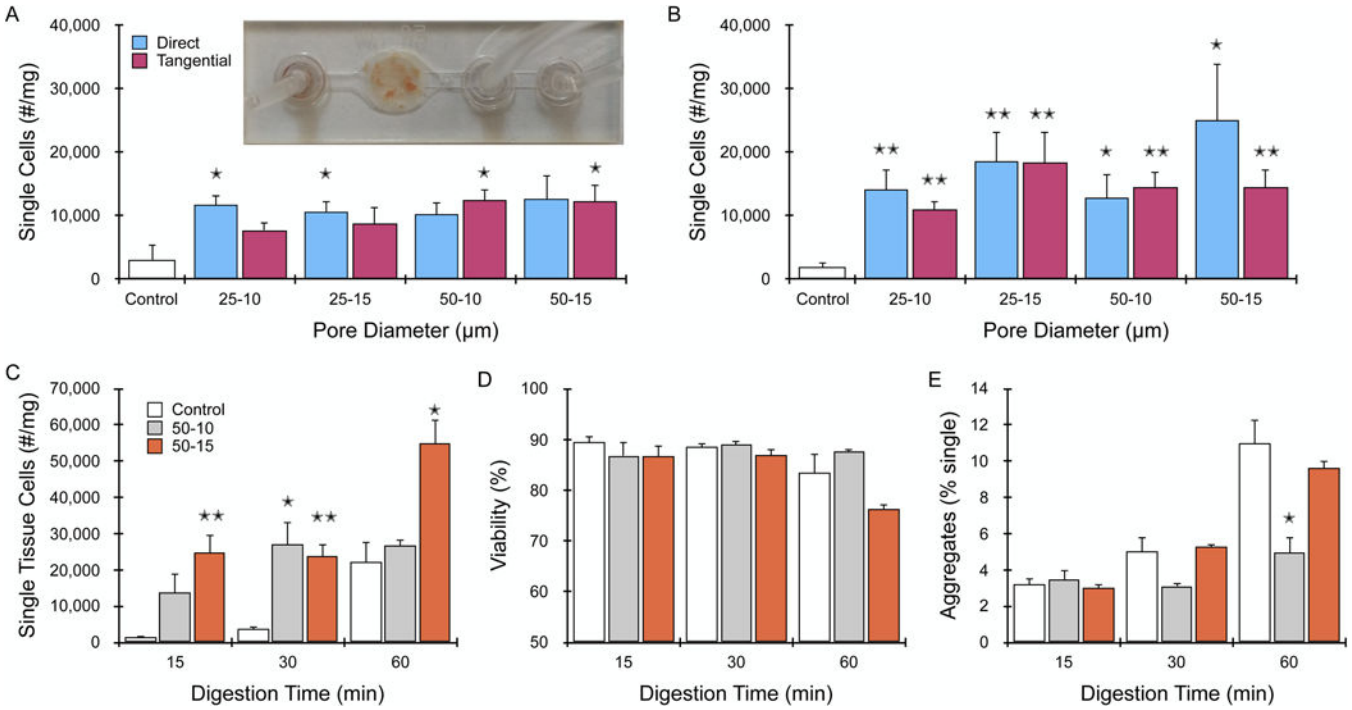

Figure 4. Optimization of membranes and operational mode using murine kidney tissue.

Freshly harvested kidney tissue was minced and digested with collagenase before passing through the two filter devices that were coupled in series. (A-B) Evaluation of the 25 or 50 μm membranes combined with the 10 or 15 μm membranes, performed under direct or tangential (60% cross-flow) filtration modes. Single cell count was determined using a cell counter. (A) After 15 min digestion, device treatment increased single cell recovery by 2- to 4-fold for all membrane combinations and filtration modes. Inset shows tissue captured on a 50 μm pore size membrane. (B) Device treatment increased single cell recovery by more than 5-fold for all cases after 30 min digestion. Results were generally based on the second membrane pore size, and did not vary significantly with the first membrane pore size or filtration mode. (C-E) Investigation of the 50–10 and 50–15 combinations using flow cytometry. (C) Single tissue cells numbers recovered from the 50–15 and 50–10 membrane membrane combination exceeded controls by 5- to 10-fold at the 15 and 30 min digestion times. After 60 min digestion, the 50–15 μm combination enhanced single tissue cell recovery by 2.5-fold. (D) Viability was ~90% for all conditions at the 15 and 30 min digestion times, but decreased after 60 min digestion to ~80% for the control and 75% for the 50–15 μm filter combination. (E) Aggregate and cluster numbers were quantified using scattering information and are presented relative to single cells. Aggregates increased with digestion time for controls, remained the same using the 50–15 membrane combination, but decreased for the 50–10 membrane combination. Error bars represent standard errors from at least three independent experiments. * indicates $p < 0.05$ and ** indicates $p < 0.01$ relative to the control at the same digestion time.

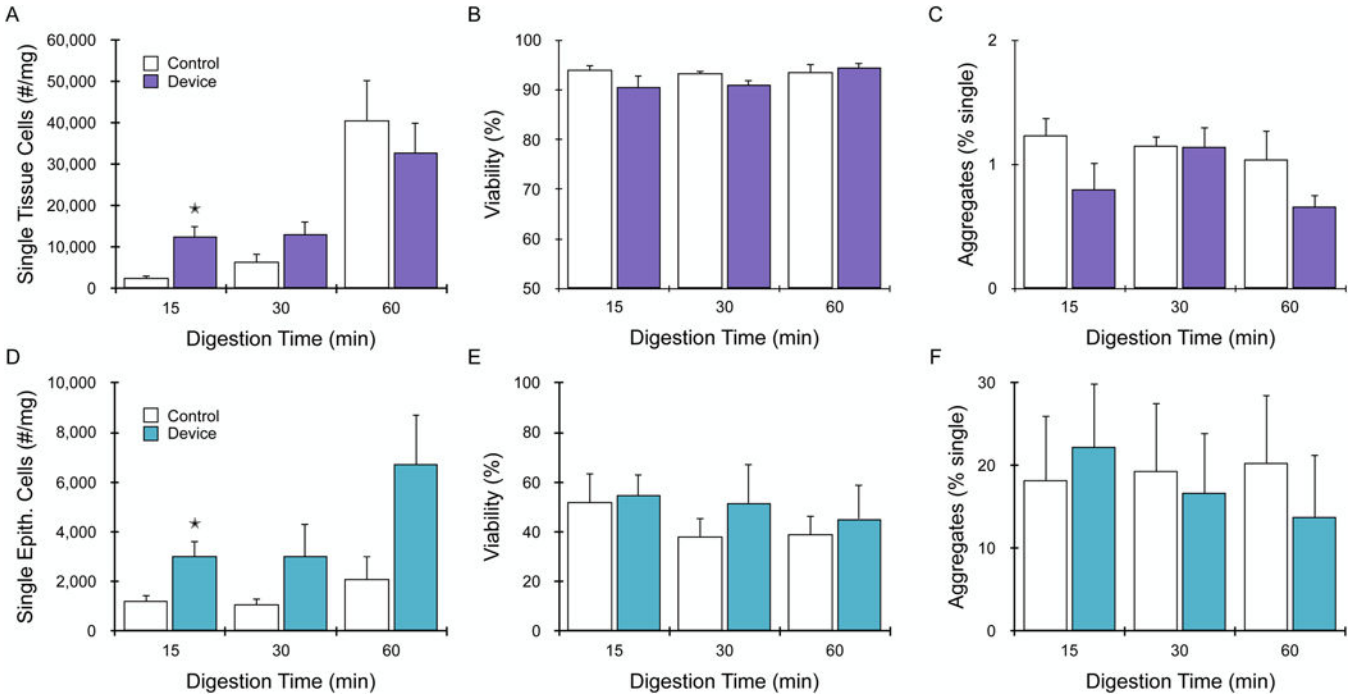

Figure 5. Validation of the integrated dual membrane filter device using murine liver and mammary tumor tissue samples.

Freshly harvested murine liver and breast tumor tissue was minced and digested with collagenase before passing through the microfluidic filter device containing 50 and 15 μm membranes. (A-C) Liver samples. (A) Device treatment increased single liver tissue cells by 5-fold and 2-fold after 15 and 30 min digestion, respectively. The device did not increase single liver tissue cells further after 60 min, as enzymatic digestion had fully liberated cells. (B) Viability remained greater than 90% for controls and device conditions. (C) Aggregates were present at ~1% for controls at all digestion times, and were generally reduced by device treatment. (D-F) Mammary tumor tissue. (D) Device treatment increased single epithelial cells by 3-fold at all digestion times. (E) Cell viability was significantly lower for tumors at 40–50%, but did not vary significantly with digestion time or device treatment. (F) Aggregates constituted about 15–20% of cell suspensions for all conditions. Error bars represent standard errors from at least three independent experiments. * indicates $p < 0.05$ and ** indicates $p < 0.01$ relative to the control at the same digestion time.

Table 1:

Nylon mesh membrane properties.

Pore Diameter (μm)	Thread Diameter (μm)	Porosity (%)
5	50	1
10	28	2
15	45	5
25	42	14
50	40	31